# Flattop pulse generation based on the combined action of active mode locking and nonlinear polarization rotation

Xiaohui Fang,[1,2,*] P. K. A. Wai,[2] Chao Lu,[2] and Jinhua Chen[3]

[1]School of Physics and Electronics Engineering, Guangzhou University, China

[2]Photonics Research Center and Department of Electronic and Information Engineering, The Hong Kong Polytechnic University, Hung Hom, Kowloon, Hong Kong

[3]Department of Physics, Agricultural University of South China, China

*Corresponding author: xhfang402@hotmail.com

Received 17 October 2013; revised 24 December 2013; accepted 29 December 2013; posted 3 January 2014 (Doc. ID 199204); published 6 February 2014

A pulse-width-tunable 10 GHz flattop pulse (FTP) train is generated based on the combined action of active mode locking and nonlinear polarization rotation pulse shaping. Although the setup was previously used for other applications, the mechanism of FTP generation based on it is first analyzed and confirmed in the experiment. An FTP with pulse width tunable from 12 to 20 ps by changing polarization controllers is generated within the wavelength tuning range of 20 nm. The generated pulse reveals good stability, with the side mode suppression ratio of 65 dB, timing jitter of 92 fs, and amplitude fluctuation of 0.36%. © 2014 Optical Society of America

*OCIS codes:* (320.5540) Pulse shaping; (140.3600) Lasers, tunable; (190.4370) Nonlinear optics, fibers.

http://dx.doi.org/10.1364/AO.53.000902

## 1. Introduction

Optical demultiplexing of a high bit rate pulse train is sensitive to the timing jitter of the pulse train used for demultiplexing. The tolerance to the timing jitter of the pulse train can be improved by using flattop pulses (FTPs) for the demultiplexing [1–3]. There are some methods for flattop or square pulse shaping. Weiner group has reported that spectral line-by-line pulse shaping can generate optical pulse with arbitrary waveform. This method uses grating combined liquid crystal modulator where intensity and phase of each spectral line can be tuned according to requirement. However, the spectral linewidth for each line should be as narrow as possible (2.6 GHz reported recently is not enough) to obtain the desired waveform [4–6]. Another drawback is the bulk structure bringing high insertion loss, big volume, and not compatible with fiber. An FTP generated based on walk-off effect in the nonlinear loop mirror needs a high-power pulse source and a cw optical source [7]. There are other reports of simple all-fiber FTP reshaping schemes that use either a superstructured fiber Bragg grating (SFBG) [1–3] or a differential long period grating (DLPG) [8] as a filter to obtain a square or FTP train. For the SFBG-based method, sinc-like spectral transfer function is designed. This pulse strategy is thus based on the proper manipulation of the spectral domain features of the input optical pulse in order to obtain the spectral profile that corresponds to the desired temporal profile. This so-called Fourier-domain approach has been extensively used in conventional optical pulse shapers based on bulk diffraction gratings [4]. Precise control of the refractive index modulation along the grating

1559-128X/14/050902-05$15.00/0

length is needed, and because it is not easy to fabricate wide bandwidth fiber Bragg grating (FBG), temporal waveform less than a few tens of picoseconds is not easy to be synthesized (the minimum pulse width reported by use of this method is 5 ps) [3]. For the DLPG-based method, an FTP is generated by use of a temporal differentiator of uniform long period grating (LPG) when it is fabricated on full coupling from core mode to cladding mode, and FTP is synthesized by input pulse fills the energy valley of two differential output Gaussian pulses when there is a proper detune between the center wavelength of the input pulse and resonance frequency of the LPG. Due to the wide transmission spectrum valley, subpicoseconds narrow pulse can be obtained [8]. The drawback of this method is that a chirp-free symmetrical Gaussian input pulse is required to obtain FTP output; another problem is the big loss for the output pulse because synthesization occurs on the transmission spectral valley of the LPG.

For all these methods, pulse shaping occurs on the optical signal, special shaping scheme needs to be designed for each signal with different central wavelength and pulse width. In this paper, we present direct generation of an FTP clock source based on the combined action of active mode locking and nonlinear polarization rotation (NPR) pulse shaping, which can be used for demultiplexing signal with different wavelength and pulse width. The laser cavity consists of two parts: one part is a commonly used actively mode-locked fiber laser, which is made up of a 10 GHz modulator, a bandpass filter, and a high-power erbium-doped fiber amplifier (EDFA). The other part is for NPR-based pulse shaping, which is composed of two polarization controllers (PCs) between which a high nonlinear fiber (HNLF) is inserted, and an in-line polarizer is inserted into the cavity to control the pulse shape. Although the setup is used as other applications of supermode suppression in erbium-doped actively mode-locked fiber lasers [9] and rational harmonic active mode locking [10,11], the mechanism of FTP generation is first analyzed and confirmed in the experiment. An FTP with the pulse width tunable from 12 to 19 ps by changing the PCs is generated, and the generated FTP is wavelength tunable within the wavelength tunable range of 20 nm. The generated pulse train also reveals good stability, with the measured side mode suppression ratio (SMSR) of 65 dB and very low timing jitter of 92 fs. The system can be used as a clock source for demultiplexing schemes.

## 2. Experimental Setup and Operation Principle

Figure 1 shows the experimental setup for FTP generation based on the combined action of active mode locking and NPR pulse shaping. On the left side of the dotted line in Fig. 1 is a common active mode locking section, which includes a Mach–Zehnder-type intensity modulator (MOD) biased at −3.4 mV and driven by a 10 GHz and 3 dBm radio-frequency (RF) sinusoidal electrical signal. A PC (PC3) is put in front of the polarization-sensitive MOD. A bandpass filter (BPF) with a 3 dB bandwidth of 6 nm is used to suppress supermode noise of the actively mode-locked laser. A variable optical delay line (VODL) is used to vary the length of the ring cavity, the delay range of the VODL is 0–330 ps, and the readout scale resolution is 0.05 mm. The EDFA used here has the maximum output power of 340 mW. On the right side of the dotted line is the NPR mechanism adopted for FTP generation, which includes two PCs (PC1 and PC2), a 1.9 m long bismuth oxide-based highly nonlinear fiber (Bi-HNLF), which has a nonlinear coefficient of 1000 $(\mathrm{Wkm})^{-1}$, and total loss of 9 dB, and an in-line polarizer.

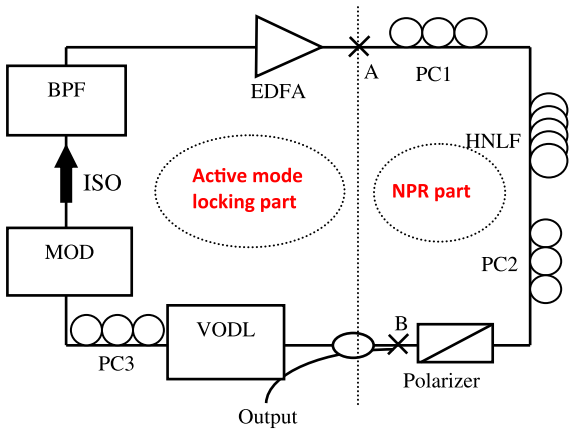


Fig. 1. Experimental setup for the FTP generation based on the combined action of active-mode-locking and NPR.

The transmission principle of the NPR mechanism is shown in Fig. 2 [11]. The input signal with electric vector E comes to the NPR part, where there exists birefringence in the Bi-HNLF, the x axis represents the fast axis of the HNLF, and the y axis the slow axis. $\alpha_1$ is the angle between the polarization direction of input pulse (the direction of electric vector E) and the x axis, and $\alpha_2$ is the angle between the x axis and polarization direction of the polarizer. The transmission introduced by NPR can be expressed as [11]

$$T = \cos^2\alpha_1 \cos^2\alpha_2 + \sin^2\alpha_1 \sin^2\alpha_2 + \frac{1}{2}\sin 2\alpha_1 \sin 2\alpha_2 \cos(\Delta\phi_L + \Delta\phi_{\mathrm{NL}}), \quad (1)$$

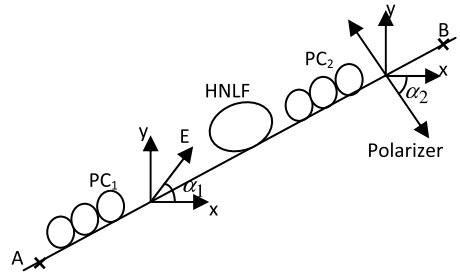


Fig. 2. Transmission principle of NPR (E, electric vector of input signal; x, fast axis of HNLF; y, slow axis of HNLF).

where $\Delta\phi_L = (n_x - n_y)\beta L, \Delta\phi_{\mathrm{NL}} = (1/3)\gamma PL \cos\alpha_2$, and $L$, $n_x$, $n_y$, $\gamma$, $P$ are the length of HNLF, linear birefringence coefficient of fast axis and slow axis, nonlinear coefficient of HNLF, and instantaneous power of input signal, respectively. $\beta = 2\pi/\lambda$, $\Delta\phi_L$ can be looked as initial phase in the cosine term in Eq. (1).

Figure 3(a) shows the principle of FTP generation in the NPR mechanism. When the actively mode-locked pulses at 10 GHz go through the NPR mechanism, they experience pulse shaping. When the peak power of pulse is higher than $P_p$, the power for peak transmission, the pulse will only experience pulse compression, which is shown in Fig. 3(a) (output pulse from point B, dashed line). However, for the pulse with peak power higher than $P_p$, the pulse shaping process is divided into two parts. For the part of the pulse with instantaneous power exceeding $P_p$, the transmission will be reduced and a flattop will then be formed, while for the other part of the pulse with instantaneous power less than $P_p$, the higher instantaneous power will lead to higher transmission, which will steepen the edges of the pulse. Finally, an FTP will be generated after NPR [Fig. 3(a), output pulse from point B, solid line]. When the peak power of the input pulse is further increased, the transmission of peak power of the pulse is reduced too much to form a flattop, a dip appears on the pulse after the NPR mechanism, which is shown in Fig. 3(a) (output pulse from point B, dotted line).

Tuning PC1 and PC2 properly to change the values of $\alpha_1$ and $\alpha_2$, and transmission curve is then changed according to Eq. (1), which results in the shape and pulse width of the output FTP being changed.

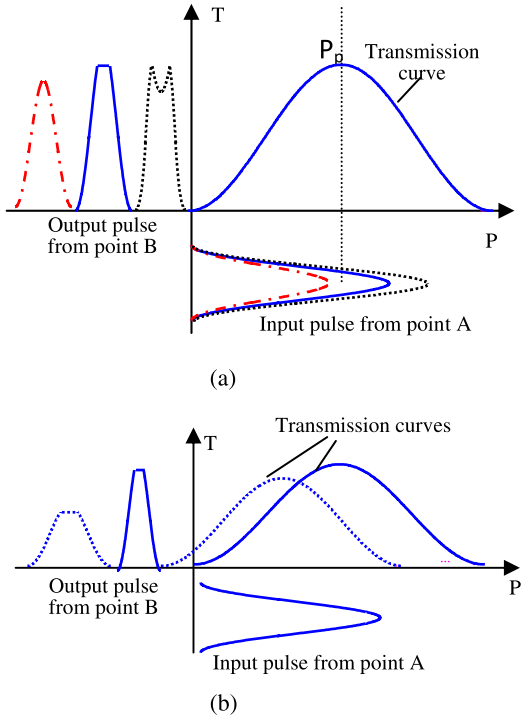


Fig. 3. (a) Principle of FTP generation and (b) principle of FTP pulse width changed with transmission curve.

Figure 3(b) shows principle of the FTP pulse width changed with the transmission curve. Two transmission curves (solid line and dotted line) correspond to two sets of $\alpha_1$ and $\alpha_2$, and the two output FTPs (solid line and dotted line) correspond to two transmission curves, respectively.

## 3. Results and Discussion

Carefully tuning three PCs in the setup to make the laser cavity work in the FTP output state, then changing the pump power of the EDFA step by step, the evolution of waveform can be observed. Figure 4 shows the evolution of the waveform by increasing the pump power of the EDFA from (a) 50 mW, (b) 120 mW, (c) 190 mW, and (d) 250 mW. The pulse is measured by optical sampling oscilloscope (OSO) (ANDO AQ7750), with ultrawide bandwidth of 700 GHz and very fast time response; the rise time of the OSO is just 100 fs. From Fig. 4(a) we can see that when the pump power is 50 mW, the pulse train only experiences compression in the NPR section and sech-like pulse is observed. This is because the peak power of the pulse train after EDFA is less than the power for maximum transmission $P_p$. When the pump power reaches to 120 mW, the peak power higher than $P_p$, FTPs can be observed, which are shown in Fig. 4(b). Further increasing pump power to 190 mW, dips on the pulse train are formed after NPR section, which is because the peak powers of the pulse train are so much higher than $P_p$ that their transmission is reduced too much to form flattop [Fig. 4(c)], which was explained and shown in Fig. 3. When the pump power reaches to 250 mW, the dips become much deeper, which is shown in Fig. 4(d).

Figures 5(a)–5(c) show the output FTP waveform with FWHM of 12.3, 15.6, and 19.1 ps, respectively (the pulses are averaged twice), and Figs. 5(d)–5(f) give the spectra corresponding to Figs. 5(a), 5(b), and 5(c), respectively. The pulse width is tunable by varying the two PCs to change the values of $\alpha_1$

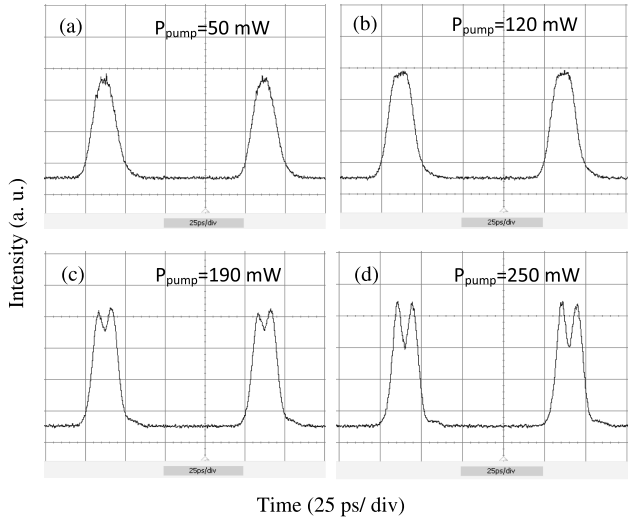


Fig. 4. Evolution of waveform by increasing pump power of EDFA from (a) 50 mW, (b) 120 mW, (c) 190 mW, and (d) 250 mW.

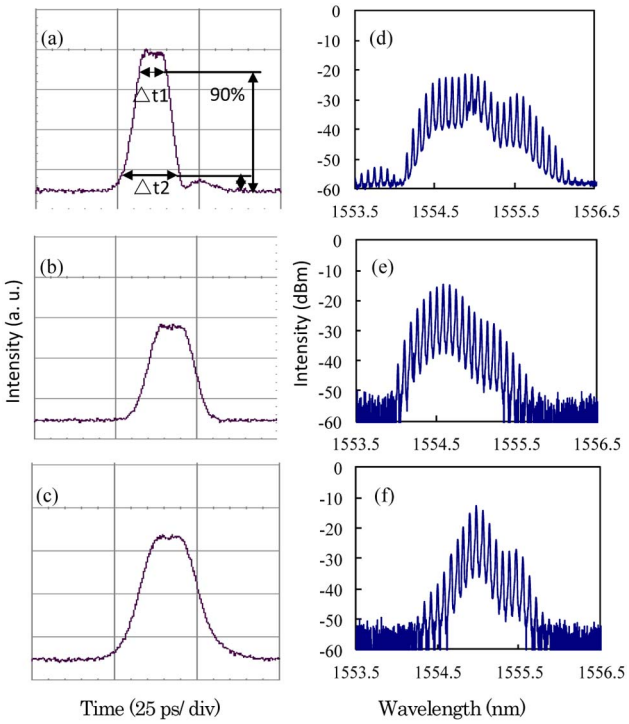


Fig. 5. (a)–(c) Output FTP trains at different polarization state and (d)–(f) the spectrum corresponding to (a), (b), and (c), respectively.

and $\alpha_2$, which in fact shifts the transmission curve of the NPR mechanism according to Eq. (1) [11].

The ratios between the pulse width at 90% and 10% of the peak power of the FTP for Figs. 5(a), 5(b), and 5(c) are 48%, 45%, and 38%, respectively. For comparison, the 90%–10% pulse width ratio for an unchirped Gaussian pulse, is only 21%, which indicates the process of pulse compression in the NPR section largely increases the steepness of the edges of FTPs. The ratio can be further optimized by changing PC1 and PC2, choosing a proper bias current and RF driving current of the modulator, or, best of all, increasing the length of the HNLF according to Eq. (1). From Figs. 5(d), 5(e), and 5(f), the bandwidth of the three different FTPs are 0.629, 0.396, and 0.209 nm, respectively. For the output FTPs, we determine the pulse chirp by comparing the spectral bandwidth of the Fourier transform of the intensity profile of the FTP with that of the measured spectrum. From Figs. 5(c) and 5(f), the calculated transform-limited and the measured time-bandwidth product are 0.2 and 0.499, respectively. The large chirp comes from the large nonlinear effect. Although the pulse generated by the proposed method contains a large chirp, the generated FTP can still be used as the optical clock source for demultiplexing schemes based on cross-gain modulation.

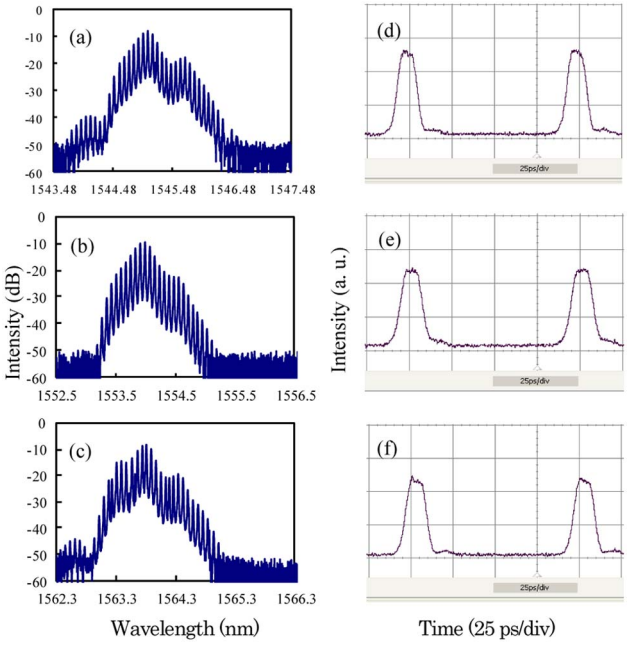


Fig. 6. Spectra of generated FTPs at different wavelengths of (a) 1545.05 nm, (b) 1553.97 nm, (c) 1563.79 nm, and (d)–(f) the waveforms corresponding to (a)–(c), respectively.

Tuning the BPF to change the filtering wavelength, and VODL, FTP also can be obtained at any other wavelength of gain bandwidth of EDFA. Figure 6 shows the spectra of generated FTPs at different wavelengths of (a) 1545.05 nm, (b) 1553.97 nm, and (c) 1563.79 nm, and corresponding waveforms of (d)–(f), respectively.

Figure 7(a) shows the measured SMSR is 65 dB, which indicates the supermode noise being very well suppressed. The reason for the supermode noise

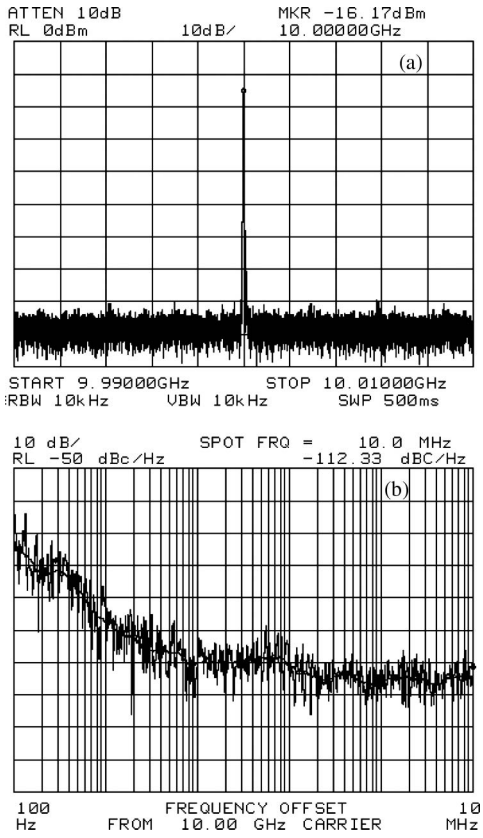


Fig. 7. Measured (a) SMSR and (b) phase noise for the output FTP.

suppression is because the NPR section acts as a "high-power pass filter," which means the lower intensity supermodes compared with the higher intensity of beat frequency at 10 GHz will experience lower transmission after the NPR section. As a result, supermode noise is suppressed very well. Figure 7(b) shows the measured phase noise curve. Through integrating operation in the RF spectrum analyzer over the entire frequency range shown in Fig. 7(b), the root mean square (RMS) phase noise $\Delta\varphi_{\mathrm{RMS}}$ is obtained to be 0.0058 rad. Then the RMS timing jitter can be calculated according to the following Eqs. [12,13]:

$$\Delta t_{\mathrm{RMS}} = \frac{\Delta\varphi_{\mathrm{RMS}}}{2\pi} T, \tag{2}$$

where $T$ is the period of the FTP. The RMS timing jitter $\Delta t_{\mathrm{RMS}}$ is calculated to be 92 fs. And we calculated that the amplitude fluctuation is about 0.36% [13]. The very high phase and amplitude stability are quite remarkable although the fiber laser is mode locked at a high harmonic.

## 4. Conclusion

We have proposed the generation of a 10 GHz FTP based on the combined action of active mode locking and NPR pulse shaping. The pulse width is tunable from 12 to 19 ps by changing PCs, and the FTP can be obtained within the wavelength range of 20 nm. The range of pulse width tunability is expected to be wider by carefully tuning PC1 and PC2. The generated FTPs reveal good stability with the measured SMSR of 65 dB, the timing jitter of 92 and amplitude fluctuation of 0.36%, which can be used as the clock source for the demultiplexing signal with different wavelength and repetition rate.

This work is funded by Natural Science Foundation of Zhejiang Province, China (grant Y1100876), Natural Science Foundation of Guangdong Province, China (grant S2013010014807), and the Fund of Guanzhou University (grant FXH1-101001).

## References

1. P. Petropoulos, M. Ibsen, A. D. Ellis, and D. J. Richardson, "Rectangular pulse generation based on pulse reshaping using a superstructured fiber Bragg grating," J. Lightwave Technol. **19**, 746–752 (2001).
2. F. Parmigiani, P. Petropoulos, M. Ibsen, and D. J. Richardson, "All-optical pulse reshaping and retiming systems incorporating pulse shaping fiber Bragg grating," J. Lightwave Technol. **24**, 357–364 (2006).
3. L. K. Oxenlowe, F. Parmigiani, M. Galili, D. Zibar, A. T. Clausen, M. Iben, P. Petropoulos, D. J. Richardson, and P. Jeppesen, "160 Gb/s retiming using rectangular pulses generated using a superstructured fibre Bragg grating," *OptoElectronics and Communications Conference/16th International Conference on Integrated Optics and Optical Fiber Communication* (Optical Society of America, 2007), paper 13B3-4.
4. A. M. Weiner, J. P. Heritage, and R. N. Thurston, "Synthesis of phase-coherent, picosecond optical square pulses," Opt. Lett. **11**, 153–155 (1986).
5. Z. Jiang, C. Huang, D. E. Leaird, and A. M. Weiner, "Optical arbitrary waveform processing of more than 100 spectral comb lines," Nat. Photonics **1**, 463–467 (2007).
6. Z. Jiang, D. E. Leaird, C. B. Huang, H. Miao, M. Kourogi, K. Imai, and A. M. Weiner, "Spectral line-by-line pulse shaping on an optical frequency comb generator," IEEE J. Quantum Electron. **43**, 1163–1174 (2007).
7. D. U. Noske, N. Pandit, and J. R. Taylor, "Picosecond square pulse generation using nonlinear fibre loop mirror," Electron. Lett. **28**, 908–909 (1992).
8. Y. Park, M. Kulishov, R. Slavík, and J. Azaña, "Picosecond and sub-picosecond flat-top pulse generation using uniform long-period fiber gratings," Opt. Express **14**, 12670–12678 (2006).
9. Y. Li, C. Lou, J. Wu, B. Wu, and Y. Gao, "Novel method to simultaneously compress pulses and suppress supermode noise in actively mode-locked fiber ring laser," IEEE Photon. Technol. Lett. **10**, 1250–1252 (1998).
10. S. Li, C. Yun, and K. T. Chan, "Rational harmonic active and passive mode locking in a figure-of-eight fiber laser," Electron. Lett. **34**, 375–376 (1998).
11. Z. Li, C. Lou, K. T. Chan, Y. Li, and Y. Gao, "Theoretical and experimental study of pulse-amplitude-equalization in a rational harmonic mode-locked fiber ring laser," IEEE J. Quantum Electron. **37**, 33–37 (2001).
12. D. von der Linde, "Characterization of the noise in continuously operating mode-locked lasers," Appl. Phys. B **39**, 201–217 (1986).
13. A. Hajimiri, S. Limotyrakis, and T. H. Lee, "Jitter and phase noise in ring oscillators," IEEE J. Solid-State Circuits **34**, 790–804 (1999).